ACS SENSORS

pubs.acs.org/acssensors Article

Smartphone DNA or RNA Sensing Using Semisynthetic Luciferase-Based Logic Device

Dalu Chang, Ki Tae Kim, Eric Lindberg, and Nicolas Winssinger*

Cite This: *ACS Sens.* 2020, 5, 807−813 Read Online

ACCESS | Metrics & More | Article Recommendations | Supporting Information

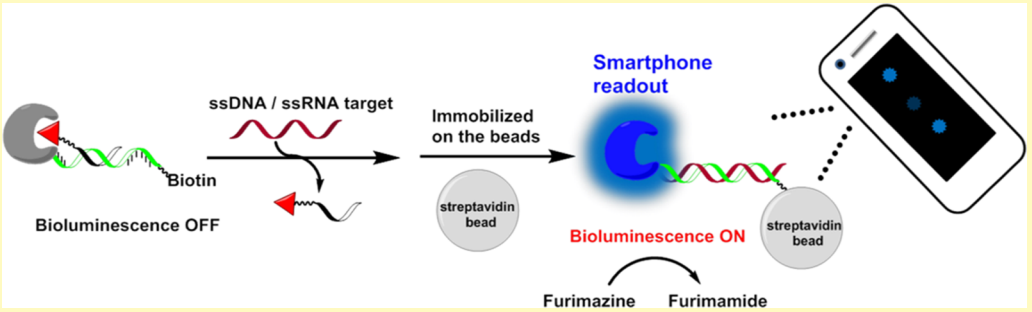

ABSTRACT: Detection of specific oligonucleotide sequences is central to numerous applications, and technologies amenable to point-of-care diagnostics or end users are needed. Here, we report a technology making use of a bioluminescent readout and smartphone quantification. The sensor is a semisynthetic luciferase (H-Luc-PNA conjugate) that is turned on by a strand-displacement reaction. We demonstrated sensing of three different microRNAs (miRs), as representative cancer biomarkers, and demonstrate the possibility to integrate an AND gate to sense two sequences simultaneously.

KEYWORDS: *biosensor, DNA, bioluminescence, PNA, smartphone readout*

Sequence specific DNA detection is central to biomedical research and at the core of applications ranging from diagnostics, forensics, environmental monitoring to food science. The demand for fast and simple readouts has inspired the development of a number of polymerase-free technologies including molecular beacons,[1,2] DNA-templated reactions,[3−7] DNA-templated split-proteins,[8,9] hybridization-chain reaction,[10] and DNA-based circuits.[11−13] Despite the tremendous progress achieved in the area, few technologies are applicable outside a laboratory setting. Pioneering reports based on light-harvesting conducting polymers[14] yielded naked-eye detection of microRNA at 10−100 nM of analyte.[15] The advent of lateral flow assay technologies for end-user diagnostics (e.g., pregnancy test) stimulated development using this platform for microRNA detection, affording a detection threshold of 0.1−50 nM.[16,17] Another important technology that facilitates a smartphone analytical readout[18] is bioluminescence-based assay.[19] Merkx and co-workers recently demonstrated the use of bioluminescence using a BRET-based molecular beacon (Figure 1).[20,21] A challenge with BRET-based technologies is the trade-off between BRET efficiency and spectral resolution between the bioluminescence and fluorophore emission, thus limiting the turn-on ratio of a sensor and its brightness. Inspired by the work of Ghadiri and co-workers with interstitially regulated proteases,[22−24] we report the use of a DNA-triggered strand-displacement reaction in a semisynthetic luciferase molecular device composed of H-Luc[25] conjugated to a PNA[26−28] sequence complementary to the analyte and an NLuc inhibitor conjugated to a partially complementary PNA that forms a complex with the sensor (Figure 1). The sensor is inhibited in the absence of analyte (off state); however, in the presence of the analyte, a specific oligonucleotide sequence, the inhibitor is dissociated by a toehold displacement resulting in a turn-on of bioluminescence.

MATERIALS AND METHODS

PNA Synthesis. PNAs were prepared by automated Mtt chemistry on an Intavis MultiPep instrument in 500 μL fritted tubes as previously described.[29] The final compounds were purified by reverse-phase chromatography using a Biotage Isolera ONE equipped with a Biotage SNAP Cartridge KP-C18-HS (linear gradient from 100% H_2O 0.01% trifluoroacetyl (TFA) to 100% MeCN 0.01% TFA with a flow rate of 5 mL/min) or using an Agilent 1100 series HPLC equipped with DAD and with a Agilent ZORBAX Eclipse XDB-C18 (4.6 × 250 mm^2, 5 μm) column (linear gradient from 100% H_2O 0.1% TFA to 100% MeCN 0.1% TFA with a flow rate of 1 mL/min). PNA sequence made use of alternating γ-modified-Ser-PNA[29] and

Received: December 11, 2019
Accepted: March 3, 2020
Published: March 3, 2020

https://dx.doi.org/10.1021/acssensors.9b02454
ACS Sens. 2020, 5, 807−813

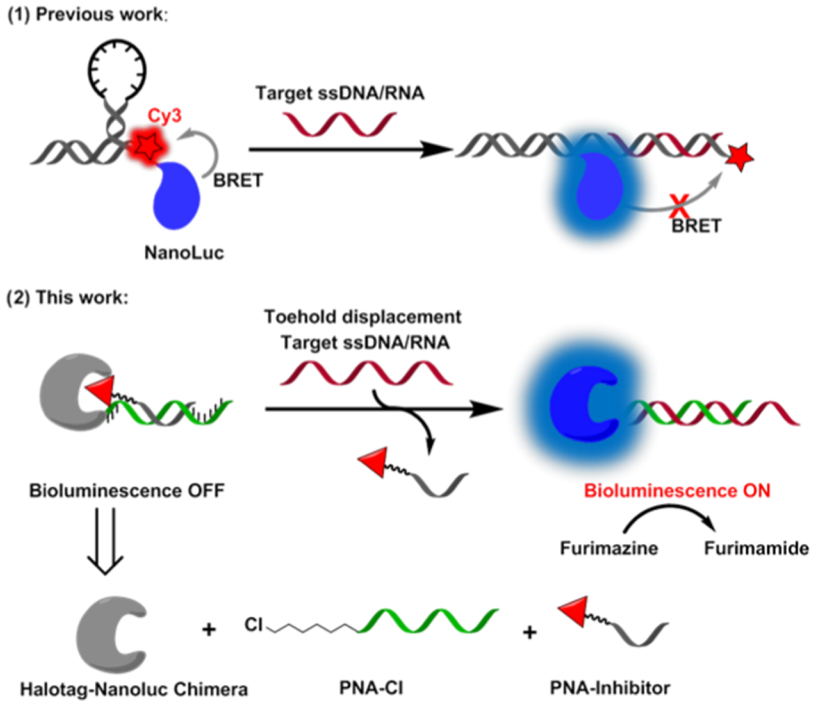

Figure 1. Schematic representation of the bioluminescent-DNA sensor. Top: previous work leveraged on changes in BRET. Bottom: this work leveraged on toehold strand displacement of the inhibitor-PNA conjugate to turn-on of the bioluminescence.

standard PNA monomers (see the Supporting Information for the detailed structure). Chloroalkane, inhibitor, and biotin were conjugated by the standard amide bond coupling procedure (HATU, DIPEA, 2,6-lutidine preactivation).

H-Luc. H-Luc was produced and purified as previously described.[30]

Sensor Preparation (H-Luc PNA-Cl Coupling). H-Luc (1 μM) and **PNA-Cl** (1 μM) were incubated in *N*-(2-hydroxyethyl)-piperazine-*N*′-ethanesulfonic acid (HEPES) buffer (50 mM HEPES, 50 mM NaCl, pH 7.2) for 1 h. The H-Luc-PNA conjugate was used without further purification, diluted to different concentrations in HEPES buffer with bovine serum albumin (BSA) (50 mM HEPES, 50 mM NaCl, 10 mg/mL BSA). The sensor was prepared either by the addition of **PNA-INH** (1 equiv) to the preformed H-Luc-PNA conjugate or by incubating H-Luc directly with the **PNA-Cl**/**PNA-INH** duplex according to the same conditions as above.

IC_{50} Determination for INH 1−4. H-Luc was diluted to 10 nM concentration in buffer with BSA (50 mM HEPES, 50 mM NaCl, pH 7.2, 10 mg/mL BSA, 100 μL) and treated with a solution of the inhibitor (100 μL, 40 μM to 2 nM, 2-fold serial dilution) in the same buffer systems as for the sensor. The mixture was incubated for 5 min, then furimazine (2 μL, 5 mM stock solution, final concentration is 50 μM) was added and luminescence intensity was measured using a Molecular Devices Spectra Max M5 microtiter plate reader. Each reaction was performed in triplicates and the averages were plotted (log[inhibitor] vs bioluminescence intensity, Figure 2). Curve fitting and IC_{50} determination were performed using a GraphPad Prism (curve fitting formula: [inhibitor] vs response, Y = Bottom + (Top − Bottom)/(1 + (X/IC_{50})). R^2 values of all reported curves were greater than 0.95).

Comparison of Sensors Prepared with Different PNA-INH4. H-Luc-PNA (20 nM, 100 μL) in buffer (50 mM HEPES, 50 mM NaCl, pH 7.2, 10 mg/mL BSA, 100 μL) was incubated with 1 equiv **PNA-INH4** (5−10merPNA, 20 nM, 100 μL, same buffer as H-Luc). After 1 h incubation, furimazine was added (2 μL, 5 mM stock solution, final concentration is 50 μM) and the bioluminescence intensity was measured using a Molecular Devices Spectra Max M5 plate reader. The strand-displacement reactions were carried out according to the same procedure starting from H-Luc-PNA/**PNA-INH4** and adding 1 equiv of DNA, incubating for 1 h prior to furimazine addition. Each reaction was performed in triplicates. The luminescence measurements of each condition were plotted as shown in Figure 3.

Kinetic Measurement. The kinetics of PNA-inhibitor hybridizations and strand-displacement reactions were performed as follows. The kinetics of PNA-inhibitor hybridization: 10 or 1 nM H-Luc-PNA (50 mM HEPES, 50 mM NaCl, pH 7.2, 10 mg/mL BSA, 200 μL) was incubated with 1 equiv **PNA-INH4**. At the stated time points, furimazine was added (2 μL, 5 mM stock solution, final concentration is 50 μM) and the bioluminescence intensity was measured immediately using a Molecular Devices Spectra Max M5 plate reader. The kinetics of strand-displacement reaction: 10 or 1 nM H-Luc-PNA was incubated with 1 equiv **PNA-INH4** for 1 h, then 1 equiv of DNA was added. At the stated time points, furimazine was added (2 μL, 5 mM stock solution, final concentration is 50 μM) and the bioluminescence intensity was measured immediately by Molecular Devices Spectra Max M5. All data points were measured in triplicates. The luminescence intensities were plotted as a function of time (Figure 4). The second-order rate constants were derived from curve fitting using GraphPad Prism using the following equation $Y = (Y_0 - \text{Plateau}) \times \exp(-K \times X) + \text{Plateau}$.

Sensor Assay in Solution. All procedures were performed at room temperature (ca. 20−23 °C). The sensor (H-Luc-PNA/**PNA-INH4**, 20 or 2 nM, 100 μL) in buffer (50 mM HEPES, 50 mM NaCl, pH 7.2, 10 mg/mL BSA) was treated with DNA (0.01−4.0 equiv, 100 μL, same buffer as sensor) and the mixture was incubated for 1 h. The reactions were treated with furimazine (2 μL, 5 mM stock solution, final concentration is 50 μM) and the bioluminescence intensity was measured using a Molecular Devices Spectra Max M5 plate reader. All reactions were performed in triplicates. The luminescence intensities were plotted as a function of DNA concentration (Figure 5). The limit of detection is calculated based on the three standard deviations (3σ) of the data point without analyte. The reactions in serum were performed according to the same procedure diluting the sensor and the analyte in serum (Figure 6).

Sensor Assay with Smartphone Readout. All procedures were performed at room temperature (ca. 20−23 °C). A 1 μM solution of the sensor, prepared as stated above, was diluted into the analyte solution (50 mM HEPES, 50 mM NaCl, pH 7.2, 10 mg/mL BSA) to

https://dx.doi.org/10.1021/acssensors.9b02454
ACS Sens. 2020, 5, 807−813

a final concentration of 1 nM (200 μL) in an Eppendorf tube. After 1 h, streptavidin beads (2 μL, Dynabeads MyOne Streptavidin C1, Thermo Fisher) were added and the mixture was further incubated for 1 h. Furimazine was added (2 μL, 5 mM stock solution, final concentration is 50 μM), the beads were pelleted down (Vortex micro-spin), and the luminescence was measured by smartphone photography (iPhone 11, Slow Shutter Cam, exposure time 30 s) and the RAW image was quantified using ImageJ. Images and quantification are shown in Figure 7. The sequence of miR-21: UAG CUU AUC AGA CUG AUG UUG A; DNA sequence corresponding to miR-21: TAG CTT ATC AGA CTG ATG TTG A; sequence of MM miR-21: TAG CTT ATT ACA CTG ATG TTG A; sequence of miR-31: GGCAAGAUGCUGGCAUAGC; sequence of miR-141: UAACACUGUCUGGUAAAGAUGG.

AND Gate for the Detection of Two Sequences. The sensor (8 nM) and DNA duplex (8 nM) in buffer (100 μL, 50 mM HEPES, 50 mM NaCl, pH 7.2, 10 mg/mL BSA) were treated with a solution (100 μL, same buffer as the sensor) containing the following analyte: no DNA; input 1; input 2; input 1 + 2. After 1 h, the reactions were treated with furimazine (2 μL, 5 mM stock solution, final concentration is 50 μM) and the bioluminescence intensity was measured using a Molecular Devices Spectra Max M5 plate reader. All reactions were performed in triplicates. Sensor: miR-21; DNA duplex: 5′-TAGCTTATCAGACTGATGTTG

AGTCCTAGA + 5′-TCAGTCTGATAAGCCCTAGAT + 5′-ATCG

AACTCTAGGACTCAACA; Input 1: 5′-ATCTAGGGCTTAT-CAGA

CTGA, Input 2: 5′-TGTTGAGTCCTAGAGTTCGAT.

RESULTS AND DISCUSSION

As a choice of luciferase, we opted for H-Luc, a chimera between NanoLuc (NLuc)[31] and Halo-Tag.[32] This choice is motivated by the brightness of NanoLuc, the fact that it does not require ATP for bioluminescence, and the simplicity and fast kinetics of Halo-Tag self-labeling. This chimera protein was optimized for high BRET efficiency,[25] suggesting that the catalytic site processing the furimazine substrate is close in space to the self-labeling site. This is critical since the same proximity is required for efficient inhibition of the luciferase following hybridization of the inhibitor-PNA conjugate to the semisynthetic H-Luc-PNA adduct. While DNA has been used in conjugation to halo-fusion proteins,[33,34] the reported reactions were considerably slower than small molecule substrates, which generally proceed with an apparent second-order rate constant (k_{2app}) of 10^4–10^5 M^{-1} s^{-1}. Halo-Tag has been rationally modified to enhance reactions with oligonucleotides;[35] however, adopting this strategy with H-Luc would require further protein engineering. Our own attempts to conjugate a chloroalkane-modified DNA to H-Luc afforded less than 10% conjugation after 12 h using a stoichiometric reaction at 1 μM. Gratifyingly, the conjugation of PNA proved much more efficient under stoichiometric coupling conditions. Labeling with chloroalkane-modified PNA (**PNA-Cl**, 17-mer, complementary to miR-21; see Figure S1 for detailed structures) with H-Luc at 1 μM proceeded to completion within 5 min (k_{2app} = 3.6 × 10^4 M^{-1} s^{-1} Figure S2; 5 min > 10 half-labeling times), consistent with the fast rate for chloroalkane-functionalized fluorophores.[25,30] PNAs are known to hybridize with excellent sequence discrimination,[28,36] which make them well suited for sensing applications. The reaction proved sufficiently efficient that conjugation with 1 equiv of **PNA-Cl** was sufficient and the sensor could be used without further purification. Control experiments with 2 equiv of **PNA-Cl** followed by purification of the H-Luc-PNA conjugate by size exclusion column did not improve the performance of the sensor (Figures S4 and S5).

The turn-on ratio of the sensor will be dictated by the difference in inhibition between the hybridized PNA-inhibitor (i.e., intramolecular) and displaced inhibitor (bimolecular) and requires a potency of inhibition calibrated between the effective concentration of the inhibitor in the hybridized complex and the dissociated concentration. The reported structure–activity relationship (SAR) for a series of NLuc inhibitors[37] suggested that derivatization off the thienopyrrole amide (see structure in Figure 2) points toward the solvent-exposed side of the NLuc-inhibitor complex and should tolerate conjugation with a PNA. We evaluated several permutations of inhibitor-PNA conjugates (**PNA-INH** 1–4, Figure 2) to identify the optimal potency. The inhibitors were tested at a high furimazine concentration (50 μM), which provides a long and bright luciferase glow. Under these conditions, IC_{50} ranging from 3.92 to 0.39 μM was obtained for **PNA-INH 1–4**. Importantly, the most potent inhibitor (**PNA-INH4**) showed no inhibition at 10 nM suggesting that once displaced from the sensor, the full brightness of the sensor should be recovered.

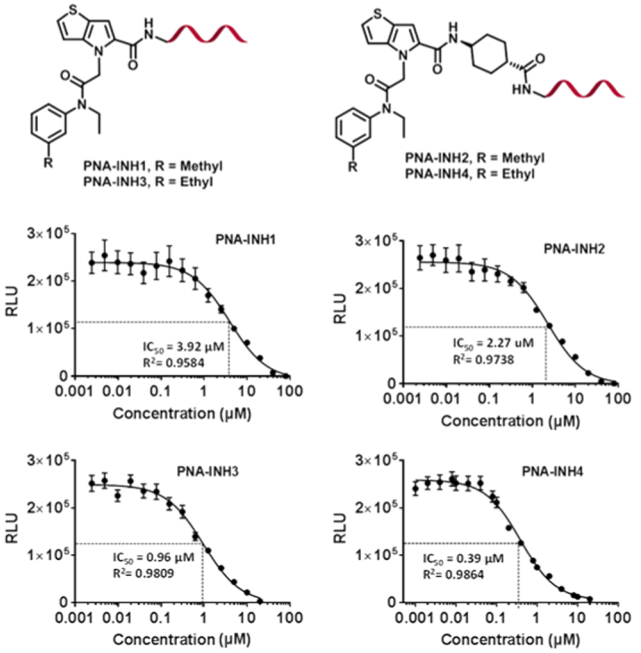

Figure 2. IC_{50} measurements of PNAs conjugated to different inhibitors. Conditions: H-Luc (5 nM) with varying concentration of PNA-inhibitor (1 nM to 20 μM), 50 μM furimazine. Error bars represent the deviation from three independent experiments.

We next tested the ability of the inhibitor to switch off the bioluminescence as a supramolecular complex at a low sensor concentration (10 nM, Figure 3). The PNA sequence of the inhibitor must be sufficiently long to ensure that the complex is formed at this concentration but not too long to offset the displacement reaction with DNA. Cooperativity between the inhibitor binding to H-Luc and PNA–PNA hybridization might provide additional stability.[38] As shown in Figure 3, the H-Luc-PNA adduct was treated with 1 equiv of inhibitor (**INH4**) conjugated to PNAs of different length (5–10-mer). Analysis from this first step indicates that there is no benefit of a 10-mer PNA over the 8-mer, both yielding 97% inhibition

https://dx.doi.org/10.1021/acssensors.9b02454
ACS Sens. 2020, 5, 807–813

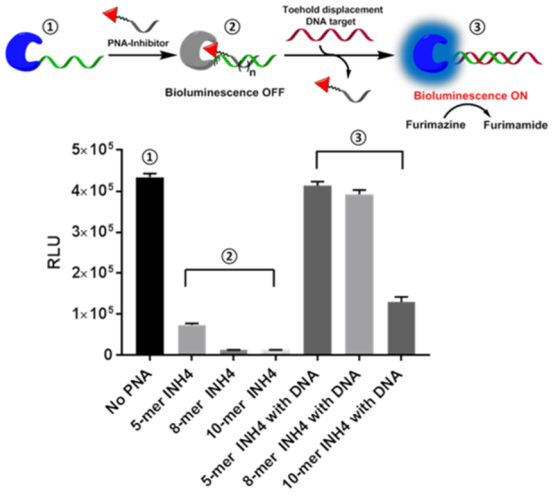

Figure 3. Efficiency of inhibition and turn-on of the sensor as a function of the length of PNA-inhibitor conjugate. Conditions: H-Luc-PNA (10 nM) in HEPES buffer with 1 equiv of **PNA-INH4** (10 nM) followed by 1 equiv of DNA (miR-21 sequence, 10 nM). Bioluminescence is measured by taking an aliquot of the solution and treating it with furimazine (50 μM final concentration). Error bars represent the deviation from three independent experiments.

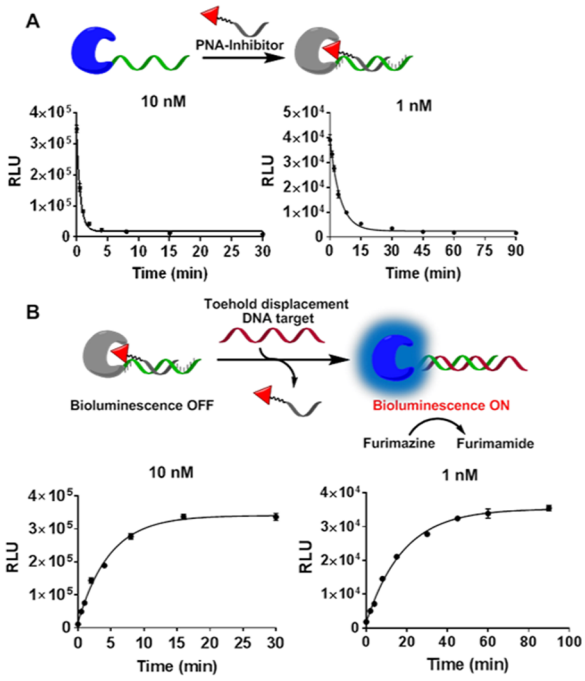

Figure 4. Kinetics of the receptor response. (A) Hybridization of the inhibitor (1 equiv) at 10 and 1 nM; (B) toehold displacement of the inhibitor with 1 equiv of analyte at 10 and 1 nM. Error bars represent the deviation from three independent experiments.

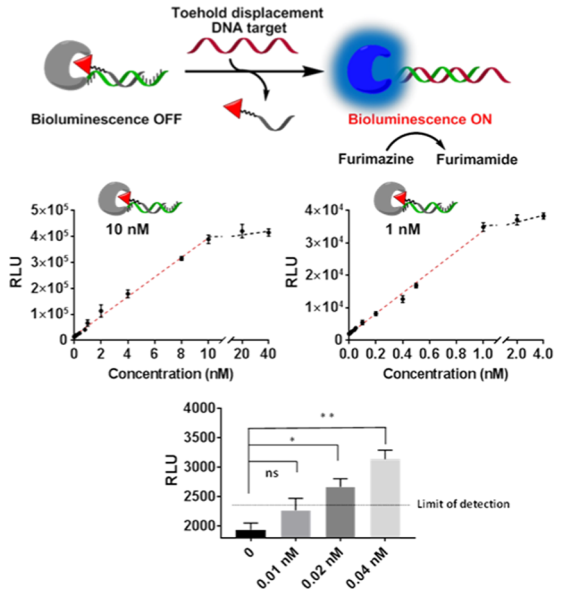

Figure 5. Dynamic range of the sensor (miR-21 sequence, 0.01–4.0 equiv; sensor at 1 or 10 nM). Error bars represent the deviation from three independent experiments. Limit of detection is set at 3σ. Stars represent paired sample *t*-test probability (*p = 0.094; **p = 0.0038).

while a 5-mer gave inferior inhibition (83%), indicating that the hybridization complex with the sensor remains dynamic. It is to be noted that all inhibitor conjugates have the same linker and hybridization position, thus the observed difference can be attributed directly to the length of the PNA. While the 5-mer PNA-inhibitor does not give complete inhibition, the level of inhibition is consistent with cooperativity between ligand binding and PNA hybridization, since the PNA itself has a K_d > 100 nM (i.e., 10-fold higher than the tested concentration).[39] Upon addition of 1 equiv of DNA (miR-21 sequence), a toehold displacement should take place and restore the activity of the sensor. Displacement of the 5-mer PNA and 8-mer restored 95 and 90% bioluminescence, respectively, while the 10-mer PNA is clearly too long leading to only a 30% recovery. It should be noted that the position of hybridization on the template is also critical and requires an overhang on both sides to ensure displacement of the PNA with the DNA. The system yielding the strongest turn-on ratio was the 8-mer PNA with a 3-mer and 6-mer overhang on each side of the template, yielding a 32-fold increase in signal. While the 10-mer PNA maintains an overhang sequence on both sides, the weaker stability of a PNA–DNA duplex (17-mer) is not sufficient to completely offset the PNA–PNA duplex (10-mer). The kinetics of the sensor response is fast; the rate of hybridization is k_{2app} > 10^6 M^{-1} s^{-1} (estimated from the curve fitting of second-order kinetics, Figure 4A), while the toehold displacement proceeds with a rate constant of k_{2app} = 4.76 × 10^5 M^{-1} s^{-1} (estimated from the curve fitting of second-order kinetics, Figure 4B), which is in line with the previous report of displacements for a 6-mer toehold,[12,40] despite the greater duplex stability of PNA–PNA vs PNA–DNA. It should be noted that that the sensor–inhibitor complex is stable down to 1 nM and can be switched off and on with 1 equiv of inhibitor and 1 equiv of DNA analyte even at this low concentration (Figures 4 and S3).

The linearity of response was tested at both 10 and 1 nM sensor concentrations. As shown in Figure 5, the bioluminescence was measured following treatment of the sensor with 0.01–4.0 equiv of DNA analyte and then plotted against the analyte concentration. Analysis showed a linear response up to 1 molar equiv of the analyte followed by a marginal increase going up to 4 equiv of DNA. This marginal increase is consistent with the fact that 1 equiv of analyte results in 90% luminescence recovery (Figure 3), while a shorter PNA-inhibitor complex indicates that a 95% recovery is possible if the displacement is driven further. Analysis of the response shows a 32-fold gain in luminescence from 0 to 1 equiv of the

https://dx.doi.org/10.1021/acssensors.9b02454
ACS Sens. 2020, 5, 807–813

analyte. Analysis of low analyte concentration (1−4%) shows a statistically significant difference between 20 pM and no DNA (0.02 equiv of the analyte relative to the sensor, limit of detection > 3σ). The response of the sensor is comparable to that in serum (Figure 6), albeit, the brightness of the sensor is

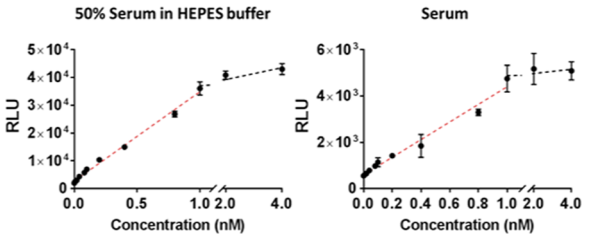

Figure 6. Response of the sensor (1 nM) to miR-21 sequence (0.01−4.0 nM) in serum (full or 50% serum in HEPES buffer). Error bars represent the deviation from three independent experiments.

diminished in full serum (50 000 RLU in serum vs 350 000 RLU in HEPES). However, full recovery of brightness can be achieved in 50% serum.

The brightness of H-Luc renders it detectable to the naked eye and smartphone camera down to 20 nM. We reasoned that the detection at the lower sensor concentration (1 nM) might still be possible if concentrated by immobilization. To this end, biotin was included in the PNA linked to H-Luc (Figure 7). Following the sensing reaction, the solution is incubated with streptavidin beads and the sensor is concentrated on the beads (100 μL of the solution concentrated on 2 μL of beads), then the beads were imaged by smartphone photography (iPhone 11, 30 s exposure time) and the intensity of the signal was quantified using ImageJ. As shown in Figure 7, this system enables detection in a semiquantitative manner of miR-21 with a detection threshold of 400 pM. The sensor clearly discriminated between microRNA-21 and a mismatch sequence (2 nucleotide mismatch) or another microRNA (miR-31). The same design, 17-mer **PNA-Cl** complementary to an miR and 8-mer **PNA-INH** complementary to **PNA-Cl** with an overhang (3- and 6-bases, respectively, on each side), was used to prepare a sensor for miR-31 (sensor 2) and miR-141 (sensor 3). As shown in Figure 7, both sensors yielded a signal increase in response to the miR and were detectable by a smartphone.

The sensor response can be integrated into different strand-displacement reactions to design a variety of logic-gated operations. To illustrate this point, we designed an AND gate that responds to the presence of two 21-nt oligonucleotide inputs (the length of an miR) but not to a single input. As shown in Figure 8, this was achieved by using a DNA strand (red strand, 30 nt) complementary to the sensor (**PNA-Cl**, green strand), which is hybridized to two masking DNAs (blue strands, 21 nt) with 6-nt overhangs. The input strands (orange) make use of toehold displacements to capture the blue strands and liberate the red strand. Optimization of the sensor had shown that overhangs were necessary on both sides of the PNA-inhibitor/**PNA-Cl** duplex to achieve a response.

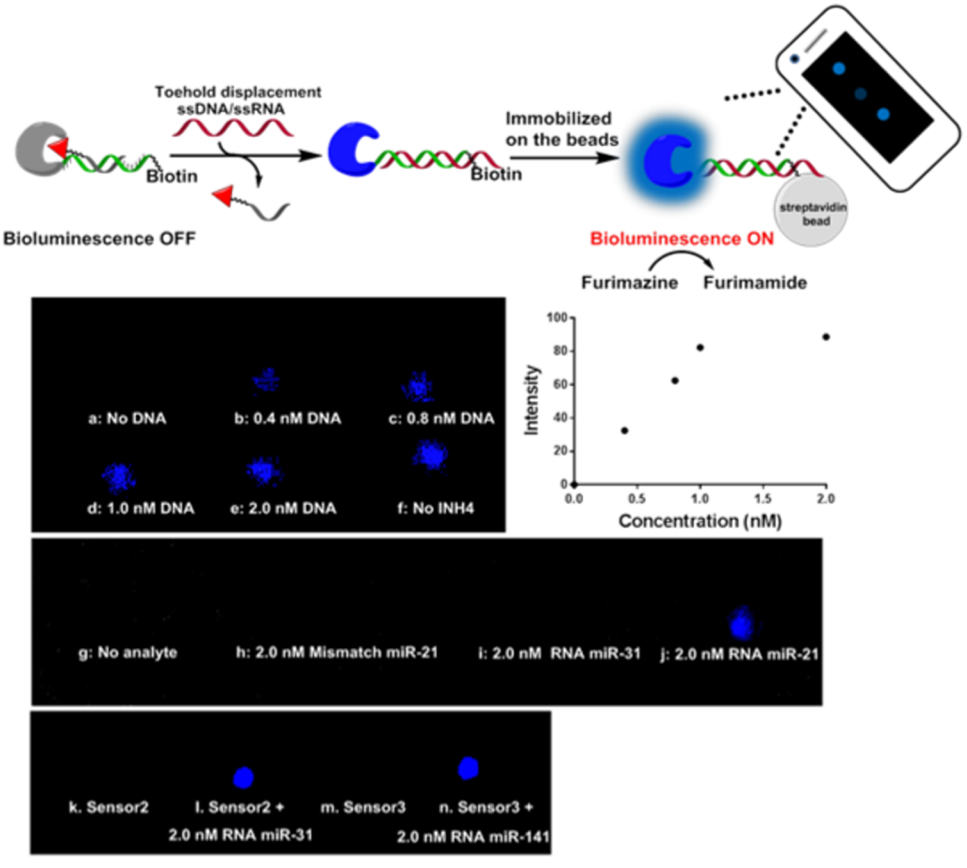

Figure 7. Nucleic acid detection by smartphone imaging. Conditions: Sensor (1 nM); streptavidin beads (2 μL); furimazine (50 μM); a−j: miR-21 sensor; k−i: miR-31 sensor; m, n: miR-141 sensor. Smartphone images were obtained with an iPhone 11 using Slow Shutter Cam (30 s exposure). The plot of intensities was prepared by quantifying signal intensity in imageJ.

https://dx.doi.org/10.1021/acssensors.9b02454
ACS Sens. 2020, 5, 807−813

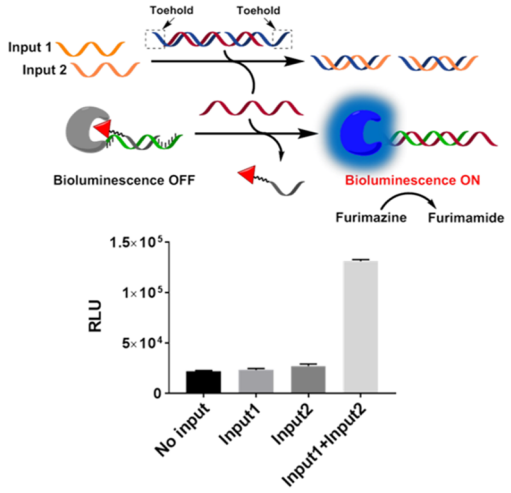

Figure 8. Sensor for two analytes (AND gate). Input 1 and input 2 (orange strand) are both necessary to release the red strand, which turns the sensor on; a single input is not sufficient to turn on the sensor. All components of the reaction (sensor, duplex, inputs) are used at 4 nM. Error bars represent the deviation from three independent experiments.

Indeed, the addition of only one input is not sufficient to achieve a response and yields a signal that is comparable to no input (Figure 8). However, in the presence of both inputs, the sensor is turned on.

CONCLUSIONS

We have demonstrated a simple mixing assay enabling sensitive detection of a microRNA sequence (miR-21, -31, -141) using smartphone imaging. Circulating miRs[41] are prominent biomarkers in serum and miR-21 in serum has been shown to correlate to tumor size,[42] while miR-31[43] and -141[44] are effective biomarkers for cancer detection. The fact that the detection of three different microRNAs (miRs) was achieved using a common design suggests that the sensor design is modular and broadly applicable to other miRs or RNAs. The technology leverages a strand displacement to control the activity of a bright luciferase (Halo-Tag–NLuc chimera: H-Luc). The sensor makes use of PNA for selective oligonucleotide recognition (DNA or RNA). This charge-neutral oligonucleotide analog also proved to be much more efficient in conjugation to Halo-Tag (H-Luc) than DNA. This work also highlights the fact that PNA duplex can be strand displaced by DNA or RNA, given there is an overhang on both sides of the displaced strand. This fact facilitates its integration in a network of strand-displacement reactions to achieve logic-gated operations (such as an AND operation).

ASSOCIATED CONTENT

Supporting Information

The Supporting Information is available free of charge at https://pubs.acs.org/doi/10.1021/acssensors.9b02454.

General conditions and analytical data for the PNA probes used; PNA probes used in all the experiments; kinetics of conjugation between PNA and H-Luc; correlation between reduction in sensor bioluminescence and stoichiometry of inhibitor at different sensor concentrations (1 and 10 nM) (PDF)

AUTHOR INFORMATION

Corresponding Author

Nicolas Winssinger − *Department of Organic Chemistry, NCCR Chemical Biology, Faculty of Science, University of Geneva 1211 Geneva, Switzerland;* orcid.org/0000-0003-1636-7766; Email: nicolas.winssinger@unige.ch

Authors

Dalu Chang − *Department of Organic Chemistry, NCCR Chemical Biology, Faculty of Science, University of Geneva 1211 Geneva, Switzerland*

Ki Tae Kim − *Department of Organic Chemistry, NCCR Chemical Biology, Faculty of Science, University of Geneva 1211 Geneva, Switzerland*

Eric Lindberg − *Department of Organic Chemistry, NCCR Chemical Biology, Faculty of Science, University of Geneva 1211 Geneva, Switzerland*

Complete contact information is available at: https://pubs.acs.org/10.1021/acssensors.9b02454

Notes

The authors declare no competing financial interest.

Raw data has been deposited on a freely accessible repository (http://doi.org/10.5281/zenodo.3689190).

ACKNOWLEDGMENTS

The authors thank the SNSF (grants: 200020_169141 and 200020_188406) and the NCCR Chemical Biology for financial support.

REFERENCES

(1) Tyagi, S.; Kramer, F. R. Molecular beacons: Probes that fluoresce upon hybridization. *Nat. Biotechnol.* **1996**, *14*, 303–308.

(2) Zhang, P.; Beck, T.; Tan, W. H. Design of a molecular beacon DNA probe with two fluorophores. *Angew. Chem., Int. Ed.* **2001**, *40*, 402–405.

(3) Xu, Y.; Karalkar, N. B.; Kool, E. T. Nonenzymatic autoligation in direct three-color detection of RNA and DNA point mutations. *Nat. Biotechnol.* **2001**, *19*, 148–152.

(4) Gorska, K.; Winssinger, N. Reactions Templated by Nucleic Acids: More Ways to Translate Oligonucleotide-Based Instructions into Emerging Function. *Angew. Chem., Int. Ed.* **2013**, *52*, 6820–6843.

(5) Choi, Y.; Metcalf, G.; Sleiman, M. H.; Vair-Turnbull, D.; Ladame, S. Oligonucleotide-templated reactions based on Peptide Nucleic Acid (PNA) probes: Concept and biomedical applications. *Bioorg. Med. Chem.* **2014**, *22*, 4395–4398.

(6) Di Pisa, M.; Seitz, O. Nucleic Acid Templated Reactions for Chemical Biology. *ChemMedChem* **2017**, *12*, 872–882.

(7) Zavoiura, O.; Resch-Genger, U.; Seitz, O. Quantum Dot-PNA Conjugates for Target-Catalyzed RNA Detection. *Bioconjugate Chem.* **2018**, *29*, 1690–1702.

(8) Furman, J. L.; Badran, A. H.; Ajulo, O.; Porter, J. R.; Stains, C. I.; Segal, D. J.; Ghosh, I. Toward a General Approach for RNA-Templated Hierarchical Assembly of Split-Proteins. *J. Am. Chem. Soc.* **2010**, *132*, 11692–11701.

(9) Sancho Oltra, N. S.; Bos, J.; Roelfes, G. Control over Enzymatic Activity by DNA-Directed Split Enzyme Reassembly. *ChemBioChem* **2010**, *11*, 2255–2258.

(10) Dirks, R. M.; Pierce, N. A. Triggered amplification by hybridization chain reaction. *Proc. Natl. Acad. Sci. U.S.A.* **2004**, *101*, 15275–15278.

(11) Qian, L.; Winfree, E. Scaling Up Digital Circuit Computation with DNA Strand Displacement Cascades. *Science* **2011**, *332*, 1196–1201.

(12) Kim, K. T.; Angerani, S.; Chang, D. L.; Winssinger, N. Coupling of DNA Circuit and Templated Reactions for Quadratic Amplification and Release of Functional Molecules. *J. Am. Chem. Soc.* **2019**, *141*, 16288−16295.
(13) Ma, F.; Zhang, Q.; Zhang, C. Y. Catalytic Self-Assembly of Quantum-Dot-Based MicroRNA Nanosensor Directed by Toehold-Mediated Strand Displacement Cascade. *Nano Lett.* **2019**, *19*, 6370−6376.
(14) Gaylord, B. S.; Massie, M. R.; Feinstein, S. C.; Bazan, G. C. SNP detection using peptide nucleic acid probes and conjugated polymers: Applications in neurodegenerative disease identification. *Proc. Natl. Acad. Sci. U.S.A.* **2005**, *102*, 34−39.
(15) Yildiz, U. H.; Alagappan, P.; Liedberg, B. Naked Eye Detection of Lung Cancer Associated miRNA by Paper Based Biosensing Platform. *Anal. Chem.* **2013**, *85*, 820−824.
(16) Sayers, J.; Payne, R. J.; Winssinger, N. Peptide nucleic acid-templated selenocystine-selenoester ligation enables rapid miRNA detection. *Chem. Sci.* **2018**, *9*, 896−903.
(17) Pavagada, S.; Channon, R. B.; Chang, J. Y. H.; Kim, S. H.; MacIntyre, D.; Bennett, P. R.; Terzidou, V.; Ladame, S. Oligonucleotide-templated lateral flow assays for amplification-free sensing of circulating microRNAs. *Chem. Commun.* **2019**, *55*, 12451−12454.
(18) Rezazadeh, M.; Seidi, S.; Lid, M.; Pedersen-Bjergaard, S.; Yamini, Y. The modern role of smartphones in analytical chemistry. *TrAC, Trends Anal. Chem.* **2019**, *118*, 548−555.
(19) Yu, Q.; Xue, L.; Hiblot, J.; Griss, R.; Fabritz, S.; Roux, C.; Binz, P. A.; Haas, D.; Okun, J. G.; Johnsson, K. Semisynthetic sensor proteins enable metabolic assays at the point of care. *Science* **2018**, *361*, 1122−1125.
(20) Engelen, W.; van de Wiel, K. M.; Meijer, L. H. H.; Saha, B.; Merkx, M. Nucleic acid detection using BRET-beacons based on bioluminescent protein-DNA hybrids. *Chem. Commun.* **2017**, *53*, 2862−2865.
(21) Meijer, L. H. H.; Joesaar, A.; Steur, E.; Engelen, W.; van Santen, R. A.; Merkx, M.; de Greef, T. F. A. Hierarchical control of enzymatic actuators using DNA-based switchable memories. *Nat. Commun.* **2017**, *8*, No. 1117.
(22) Saghatelian, A.; Guckian, K. M.; Thayer, D. A.; Ghadiri, M. R. DNA detection and signal amplification via an engineered allosteric enzyme. *J. Am. Chem. Soc.* **2003**, *125*, 344−345.
(23) Gianneschi, N. C.; Ghadiri, M. R. Design of molecular logic devices based on a programmable DNA-regulated semisynthetic enzyme. *Angew. Chem., Int. Ed.* **2007**, *46*, 3955−3958.
(24) Mukherjee, P.; Leman, L. J.; Griffin, J. H.; Ghadiri, M. R. Design of a DNA-Programmed Plasminogen Activator. *J. Am. Chem. Soc.* **2018**, *140*, 15516−15524.
(25) Hiblot, J.; Yu, Q.; Sabbadini, M. D. B.; Reymond, L.; Xue, L.; Schena, A.; Sallin, O.; Hill, N.; Griss, R.; Johnsson, K. Luciferases with Tunable Emission Wavelengths. *Angew. Chem., Int. Ed.* **2017**, *56*, 14556−14560.
(26) Egholm, M.; Buchardt, O.; Christensen, L.; Behrens, C.; Freier, S. M.; Driver, D. A.; Berg, R. H.; Kim, S. K.; Norden, B.; Nielsen, P. E. PNA Hybridizes to Complementary Oligonucleotides Obeying the Watson-Crick Hydrogen-Bonding Rules. *Nature* **1993**, *365*, 566−568.
(27) Barluenga, S.; Winssinger, N. PNA as a Biosupramolecular Tag for Programmable Assemblies and Reactions. *Acc. Chem. Res.* **2015**, *48*, 1319−1331.
(28) Saarbach, J.; Sabale, P. M.; Winssinger, N. Peptide nucleic acid (PNA) and its applications in chemical biology, diagnostics, and therapeutics. *Curr. Opin. Chem. Biol.* **2019**, *52*, 112−124.
(29) Chouikhi, D.; Ciobanu, M.; Zambaldo, C.; Duplan, V.; Barluenga, S.; Winssinger, N. Expanding the Scope of PNA-Encoded Synthesis (PES): Mtt-Protected PNA Fully Orthogonal to Fmoc Chemistry and a Broad Array of Robust Diversity-Generating Reactions. *Chem. - Eur. J.* **2012**, *18*, 12698−12704.
(30) Chang, D.; Lindberg, E.; Feng, S. H.; Angerani, S.; Riezman, H.; Winssinger, N. Luciferase-Induced Photouncaging: Bioluminolysis. *Angew. Chem., Int. Ed.* **2019**, *58*, 16033−16037.
(31) England, C. G.; Ehlerding, E. B.; Cai, W. B. NanoLuc: A Small Luciferase Is Brightening Up the Field of Bioluminescence. *Bioconjugate Chem.* **2016**, *27*, 1175−1187.
(32) Los, G. V.; Encell, L. P.; McDougall, M. G.; Hartzell, D. D.; Karassina, N.; Zimprich, C.; Wood, M. G.; Learish, R.; Ohane, R. F.; Urh, M.; et al. HatoTag: A novel protein labeling technology for cell imaging and protein analysis. *ACS Chem. Biol.* **2008**, *3*, 373−382.
(33) Saccà, B.; Meyer, R.; Erkelenz, M.; Kiko, K.; Arndt, A.; Schroeder, H.; Rabe, K. S.; Niemeyer, C. M. Orthogonal Protein Decoration of DNA Origami. *Angew. Chem., Int. Ed.* **2010**, *49*, 9378−9383.
(34) Blackstock, D.; Chen, W. Halo-tag mediated self-labeling of fluorescent proteins to molecular beacons for nucleic acid detection. *Chem. Commun.* **2014**, *50*, 13735−13738.
(35) Koßmann, K. J.; Ziegler, C.; Angelin, A.; Meyer, R.; Skoupi, M.; Rabe, K. S.; Niemeyer, C. M. A Rationally Designed Connector for Assembly of Protein-Functionalized DNA Nanostructures. *ChemBioChem* **2016**, *17*, 1102−1106.
(36) Nielsen, P. E. Peptide nucleic acid. A molecule with two identities. *Acc. Chem. Res.* **1999**, *32*, 624−630.
(37) Walker, J. R.; Hall, M. P.; Zimprich, C. A.; Robers, M. B.; Duellman, S. J.; Machleidt, T.; Rodriguez, J.; Zhou, W. H. Highly Potent Cell-Permeable and Impermeable NanoLuc Luciferase Inhibitors. *ACS Chem. Biol.* **2017**, *12*, 1028−1037.
(38) Machida, T.; Novoa, A.; Gillon, E.; Zheng, S. S.; Claudinon, J.; Eierhoff, T.; Imberty, A.; Romer, W.; Winssinger, N. Dynamic Cooperative Glycan Assembly Blocks the Binding of Bacterial Lectins to Epithelial Cells. *Angew. Chem., Int. Ed.* **2017**, *56*, 6762−6766.
(39) Chang, D.; Lindberg, E.; Winssinger, N. Critical Analysis of Rate Constants and Turnover Frequency in Nucleic Acid-Templated Reactions: Reaching Terminal Velocity. *J. Am. Chem. Soc.* **2017**, *139*, 1444−1447.
(40) Zhang, D. Y.; Winfree, E. Control of DNA Strand Displacement Kinetics Using Toehold Exchange. *J. Am. Chem. Soc.* **2009**, *131*, 17303−17314.
(41) Mitchell, P. S.; Parkin, R. K.; Kroh, E. M.; Fritz, B. R.; Wyman, S. K.; Pogosova-Agadjanyan, E. L.; Peterson, A.; Noteboom, J.; O'Briant, K. C.; Allen, A.; et al. Circulating microRNAs as stable blood-based markers for cancer detection. *Proc. Natl. Acad. Sci. U.S.A.* **2008**, *105*, 10513−10518.
(42) Toiyama, Y.; Takahashi, M.; Hur, K.; Nagasaka, T.; Tanaka, K.; Inoue, Y.; Kusunoki, M.; Boland, C. R.; Goel, A. Serum miR-21 as a Diagnostic and Prognostic Biomarker in Colorectal Cancer. *J. Natl. Cancer Inst.* **2013**, *105*, 849−859.
(43) Ma, Y.; Chen, Y. F.; Lin, J. B.; Liu, Y.; Luo, K.; Cao, Y.; Wang, T. Q.; Jin, H. W.; Su, Z.; Wu, H. L.; et al. Circulating miR-31 as an effective biomarker for detection and prognosis of human cancer: a meta-analysis. *Oncotarget* **2017**, *8*, 28660−28671.
(44) Cheng, H.; Zhang, L. N.; Cogdell, D. E.; Zheng, H.; Schetter, A. J.; Nykter, M.; Harris, C. C.; Chen, K. X.; Hamilton, S. R.; Zhang, W. Circulating Plasma MiR-141 Is a Novel Biomarker for Metastatic Colon Cancer and Predicts Poor Prognosis. *PLoS One* **2011**, *6*, No. e17745.

https://dx.doi.org/10.1021/acssensors.9b02454
ACS Sens. 2020, 5, 807−813